Microporous and Mesoporous Materials 257 (2018) 128–134

Contents lists available at ScienceDirect

Microporous and Mesoporous Materials

journal homepage: www.elsevier.com/locate/micromeso

Alkane/alkene mixture diffusion in silicalite-1 studied by MAS PFG NMR

Nina Dvoyashkina [a], Dieter Freude [a, *], Alexander G. Stepanov [b, c], Winfried Böhlmann [a], Rajamani Krishna [d], Jörg Kärger [a], Jürgen Haase [a]

[a] Faculty for Physics and Earth Sciences, Leipzig University, Linnéstr. 5, 04103 Leipzig, Germany
[b] Boreskov Institute of Catalysis, Siberian Branch of Russian Academy of Sciences, Prospekt Akademika Lavrentieva 5, Novosibirsk, 630090, Russia
[c] Novosibirsk State University, Pirogova Str. 2, Novosibirsk, 630090, Russia
[d] Van't Hoff Institute for Molecular Sciences, University of Amsterdam, Science Park 904, 1098, XH Amsterdam, The Netherlands

ARTICLE INFO

Article history:
Received 20 June 2017
Received in revised form
23 July 2017
Accepted 10 August 2017
Available online 12 August 2017

ABSTRACT

The diffusivity of *n*-alkanes and *n*-alkenes (C2 to C6) and their mixtures in silicalite-1 was studied by magic-angle spinning pulsed field-gradient nuclear magnetic resonance (MAS PFG NMR) at the temperatures of 273 K, 313 K and 373 K. It could be proved that there is no significant difference between the diffusivities of alkanes, alkenes and their mixtures for equal carbon numbers and equal total loading. The diffusivities of the alkanes, alkenes and their mixtures are found to monotonically decrease with increasing carbon number, in agreement with the results obtained in MD simulations with *n*-alkanes in silicalite-1.

1. Introduction

Sorption and diffusion of *n*-alkanes in zeolites of MFI type were widely investigated since the systems are involved in significant industrial processes, such as hydrocarbon separation, catalytic cracking and dewaxing. First investigations concerning the dependence of the intracrystalline self-diffusivity on the loading were performed by the pulsed field-gradient (PFG) NMR technique by Caro et al. [1] in 1985. Interactions between the *n*-alkane molecules and the zeolitic framework of the aluminum-free silicalite-1 are non-specific and can be modelled in dependence on the number of carbon atoms with a relatively low degree of uncertainty by molecular dynamic simulations, see, for example, Jobic and Theodorou [2] and Krishna and van Baten [3]. Separation applications of nanoporous materials are influenced by the different diffusivities of different kinds of molecules within the pores, see Krishna [4,5]. Some metal–organic framework (MOF) adsorbents like CPO-27 and ZIF-8 are, respectively, olefin and paraffin selective [6]. Magic-angle spinning (MAS) NMR diffusometry was applied for the study of the ethane/ethene mixture diffusion in ZIF-8 [7], and it was shown that the diffusivity of ethene in a one-to-one mixture is about five times higher than the diffusivity of ethane in a temperature range from 283 K to 363 K and for a total loading of 4 or 8 molecules per cavity. The aluminum-free silicalite-1 has a non-polar framework, opposite to the ZIF-8. The present contribution studies the diffusivities of *n*-alkanes and *n*-alkenes as single molecules and in binary *n*-alkane/*n*-alkene mixtures in silicalite-1 in a broad range of carbon atoms by MAS PFG NMR. The combination of MAS with PFG NMR technique has, in comparison with conventional PFG NMR, the advantage of enhanced spectral resolution for distinguishing between several compounds and the disadvantage of a reduced pulsed field gradient strength [8–12].

2. Experimental

2.1. Silicalite-1 synthesis and treatment

Silicalite-1 was synthesized according to the following procedure: 10.42 g of colloidal SiO_2 (Ludox-AS-30, DuPont) was added to a solution of 5.11 g tetrapropylammonium bromide (Aldrich) in 9.92 g distilled water and stirred at room temperature. After 15 min 24.75 ml of an aqueous solution of ammonia (25 wt. %) was added to the gel which was vigorously stirred for 5 min. The fluid gel was heated at 453 K in Teflon-lined stainless-steel autoclaves for 7 days under autogenous pressure. The obtained reaction product was intensively washed with distilled water, filtered and dried.

* Corresponding author.
E-mail address: freude@uni-leipzig.de (D. Freude).

http://dx.doi.org/10.1016/j.micromeso.2017.08.015
1387-1811/

Calcination in air for 12 h at 873 K removed the organic template. The catalytic activity of the zeolite was decreased by a hydrothermal healing procedure, see Chap. 1 in Supplementary Material. The size of the silicalite-1 crystallites varies in the range (20–40) μm × (25–50) μm × (100–200) μm, see Fig. 1.

2.2. Sample preparation

The samples for the NMR measurements were outgassed (activated) by heating 25 mg of the silicalite-1 sample in a glass tube of 3 mm outer diameter and a height of 15 mm between bottom and first capillary of the glass tube, see Chapt. 2 in Supplementary Material. The temperature increased at a rate of 50 K h^{-1} up to 673 K and remained at this temperature for 48 h with a vacuum of about 10^{-2} Pa. After cooling down to room temperature, the samples were loaded by freezing the guest molecules from a calibrated loading volume with an appropriately chosen gas pressure and sealed off, see Chap. 2 in Supplementary Material. We used 1-alkenes or 2-alkenes for the loading. A mixture of 1-alkenes and alkenes with other double bond positions occurs in our sample, since a double bond shift reaction takes place, see Chapt. 4 in Supplementary Material.

2.3. NMR measurements

NMR measurements were performed on a Bruker AVANCE 750 spectrometer at 17.6 T with a wide-bore MAS gradient probe and a MAS frequency of 10 kHz. This rotation frequency of the 4-mm MAS-rotor increases the temperature within the rotor by 10° compared to the detected temperature of the air flow outside the rotor [13]. The temperatures mentioned in Results are temperatures within the rotor. ^{1}H MAS NMR spectroscopy was done using a Hahn echo, a 16-phase cycle and a delay of one rotation period (100 μs) between π/2- and π-pulses. Pulse durations correspond to a nutation frequency of about 100 kHz also in the MAS PFG experiments. ^{1}H MAS NMR diffusometry was performed by a stimulated spin-echo sequence with eddy current delay, two sine-shaped bipolar gradient pulse pairs and two gradient quench pulses. Details are presented in Chapt. 5 in Supplementary Material. The field gradient was calibrated by a MAS PFG experiment on a fused water sample at a low rotation frequency of 4 kHz, in order to avoid vortex in the sample. The self-diffusion coefficient D of water at a temperature of 303 K is $D = 2.594 \times 10^{-9}$ m^2s^{-1} [14]. The obtained gradient strength at 100% gradient intensity is 0.54 T m^{-1}. The repetition delay was always longer than the fivefold of the longitudinal relaxation time. We used 5 s for safety of the gradient coils in the case of MAS PFG experiments. The NMR signal separation is described in Chap. 3 of Supplementary Material.

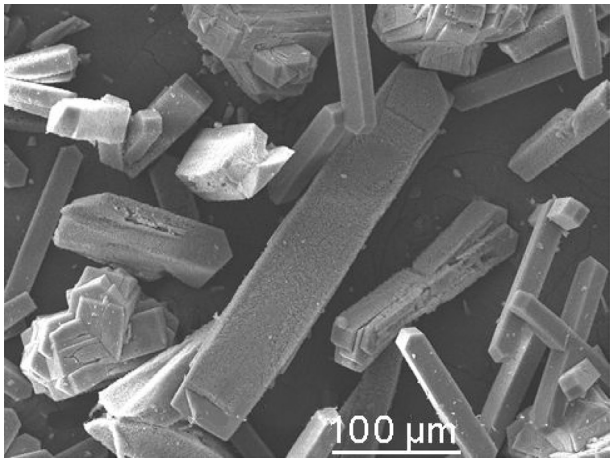

Fig. 1. SEM image of the synthesized silicalite-1 material.

2.4. PFG NMR signal attenuations

Signal decay in PFG NMR diffusion measurements is described in Chap. 5 of Supplementary Material. In the ideal case of normal, isotropic diffusion, the self-diffusion coefficient, D, of molecules is obtained from the decay of the amplitude, S, of the signal intensity, ψ, in dependence on the squared field gradient intensity, g^2, by the mono-exponential equation [12].

$$\psi\left(g^2\right) = \frac{S(g^2)}{S_0} = \exp\left[-D\left(\frac{4\delta g\gamma}{\pi}\right)^2\left(\Delta - \frac{\tau}{2} - \frac{2\delta}{3} - p_\pi\right)\right] = \exp\left[-D\left(\frac{4\delta g\gamma}{\pi}\right)^2 \Delta'\right], \quad (1)$$

in the case of a stimulated spin-echo sequence with eddy current delay, two sine-shaped bipolar gradient pulse pairs with the duration δ for a single pulse and the intensity g. The delay τ denotes the time between gradient and RF pulses. The observation time of the diffusion, Δ, is the time span between the starts of the two gradient pairs. The corrected observation time Δ', is defined by Eq. (1). The values of Δ' are in our experiments about 0.5–1.5 ms shorter than the values Δ. We use Δ' in Eqs. (1), (5) and (6), but use Δ instead of Δ' in all other cases, where the difference can be neglected. S_0 denotes the value of the amplitude for a zero-gradient. The magnetogyric ratio, γ, amounts for ^{1}H nuclei $\gamma = 26.7522128 \times 10^7$ $s^{-1}T^{-1}$. The duration of a π pulse is denoted as p_π.

Eq. (1) describes the isotropic one-component diffusion. The signal decay in dependence on the squared field gradient is more complicated for diffusion anisotropy, see Chapt. 5 of Supplementary Material, and for a superposition of the intracrystalline self-diffusion process by an intercrystalline diffusion of the molecules. The latter becomes remarkable, if the root-mean-square displacement, $\sqrt{l^2}$, within the observation time of the diffusion Δ, is not very small compared to the size of the crystallites. We get from Einstein's equation with the mean-square displacement, l^2,

$$D = l^2/6 \quad \rightarrow \quad \sqrt{l^2} = \sqrt{6\,D}. \quad (2)$$

Fig. 1 shows that the maximum size (distance of two opposite crystallite surfaces) of the crystallites is 200 μm, but the minimum size is around 20 μm. Consequently, a superimposed intercrystalline diffusion decay can be observed, if $\sqrt{l^2}$ is not very small compared to 20 μm.

An intercrystalline space exists even after a tight packing under MAS conditions, where the radial acceleration of the powder in the rotor is several hundred-thousand times greater than the standard acceleration. Therefore, a fast diffusion of molecules can proceed via the gas phase, see chapter 11 in Ref. [15]. Thus, for observation times notably longer than the intracrystalline mean life times, the diffusion path length appearing in Eq. (2) includes displacements in both the intracrystalline and intercrystalline spaces. The coefficient of overall, i.e. of “long-range” self-diffusion is then given by the relation

$$D_{\text{long-range}} = p_{\text{inter}}\, D_{\text{inter}} + (1 - p_{\text{inter}})\, D_{\text{intra}}\,, \quad (3)$$

with D_{inter} and D_{intra} denoting, respectively, the self-diffusivities in the inter- and intracrystalline spaces as resulting by

application of Eq. (2) to displacements in exclusively the respective spaces p_{inter} stands for the relative portion of molecules in intercrystalline space, see chapter 11 in Ref. [15]. It must be remarked, in passing, that the magnitude D_{intra} as appearing in this relation does not necessarily coincide with the coefficient of genuine intracrystalline diffusion, see Refs. [16,17]. It must rather be taken into account that, notably for $p_{inter}\, D_{inter} \ll D_{intra}$, subsequent displacements in the intracrystalline space are often countercorrelated, namely on molecular encounters with the crystal surface which are more likely followed by displacements into exactly the opposite direction [16,17]. For practical purposes, it is therefore completely sufficient to consider only the contribution of the first term on the right-hand side of Eq. (3) for determining long-range diffusivities. Note that this restriction ceases to exist in the opposite limiting case of intracrystalline mean life times significantly larger than the observation times since now the influence of anticorrelations in molecular displacement by encounters with the crystal surface may be implied to be negligibly small [16,17].

For covering the transition range between the limiting cases of fast and slow exchange we may substitute the isotropic one-component self-diffusion coefficient, D, in Eq. (1) by the relation

$$D_{intra} + \frac{p_{inter}\, D_{inter}}{\left(\frac{4\delta g\gamma}{\pi}\right)^2 \tau_{intra}\, p_{inter}\, D_{inter} + 1}, \qquad (4)$$

where τ_{intra} denotes the mean residence time of a molecule in one crystallite, see Eq. (11.41) in Ref. [15]. From Eqs. (1) and (4) follows

$$\ln\psi\left(g^2\right) = -\left(D_{intra} + \frac{p_{inter} D_{inter}}{\left(\frac{4\delta g\gamma}{\pi}\right)^2 \tau_{intra} p_{inter} D_{inter} + 1}\right)\left(\frac{4\delta g\gamma}{\pi}\right)^2 \Delta'. \qquad (5)$$

Eq. (5) includes mono-exponential decays in the two limiting cases of (a) long-range diffusion for $\Delta \gg \tau_{intra}$ and $p_{inter} D_{inter} \gg D_{intra}$ and (b) intracrystalline diffusion for $\Delta \ll \tau_{intra}$.

In the limit of sufficiently large field gradient intensities (i.e. for large values of g and, hence, of $\left(\frac{4\delta g\gamma}{\pi}\right)^2 \tau_{intra} p_{inter}\, D_{inter} \gg 1$) Eq. (5) simplifies to

$$\lim_{g\to\infty}\left(\ln\psi\left(g^2\right)\right) = -\left(\frac{1}{\tau_{intra}} + \left(\frac{4\delta g\gamma}{\pi}\right)^2 D_{intra}\right)\Delta'. \qquad (6)$$

Let us recollect that best agreement between the values of D_{intra} as appearing in Eqs. (5) and (6) and the genuine intracrystalline self-diffusivity is always attained for molecular displacements much less than the particle size, corresponding with molecular intracrystalline mean life times notably exceeding the observation time.

3. Data analysis

Fig. 2 shows room temperature ^{1}H MAS NMR spectra of the *n*-hexane/*n*-hexene samples. The double bond shift reaction is visible by comparing spectra 2c and 2d. We used 1-hexene for the loading, kept the sample for a few hours at room temperature and measured then spectrum 2c. One can see in the double-bond region (from 4 to 7 ppm) two strong signals at 5.8 ppm (CH-group) and two non-resolved signals at 4.8 and 5.0 ppm (terminal methylene group). Both signals belong to 1-hexene. The signal at 5.4 ppm is very weak in the spectrum 2c. It becomes dominant in spectrum 2d, which we acquired after a diffusion experiment lasting for one hour at 373 K.

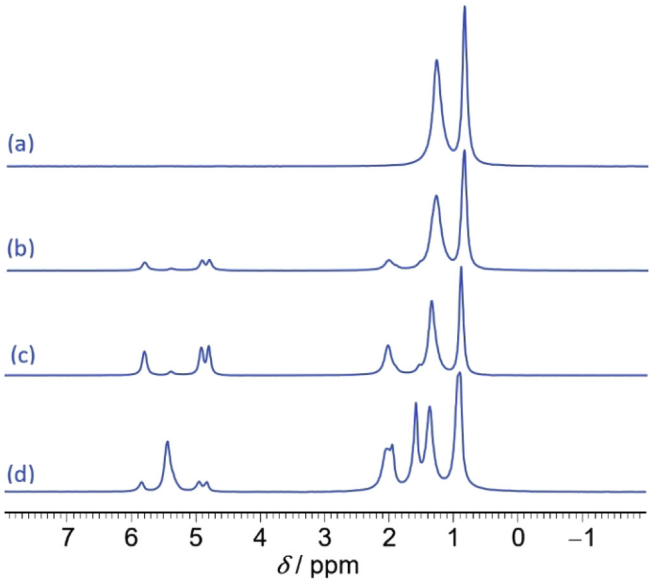

Fig. 2. ^{1}H MAS NMR spectra of *n*-hexane and *n*-hexene in silicalite-1 at the room temperature. Spectrum (a) shows the signals of *n*-hexane, (b) an *n*-hexane/*n*-hexene mixture (60%/40%). The *n*-hexene spectrum (c) was acquired a few hours after sample preparation and shows signals of *n*-1-hexene (91%) und *n*-2-hexene (9%). Spectrum (d) shows the spectrum of the same sample after keeping it for one hour at 373 K. It consists of 25% *n*-1-hexene and 75% *n*-2-hexene.

The 5.4-ppm signal belongs to two CH-groups in 2-hexene or 3-hexene. The resolution is not sufficient for distinguishing between 2-hexene and 3-hexene molecules.

The spectra show the lines for 3 or 2 hydrogen atoms in the double-bond region for 1-hexene and 2-hexene, respectively. The other hydrogen atoms of the hexene molecule give signals in the single-bond region (from 0 ppm to 3 ppm) and overlap with the signals of the *n*-hexane molecule, as can be seen in Fig. 2. This causes a problem in the processing of the diffusion spectra for the *n*-hexane/*n*-hexene mixture. We could overcome this by subtracting a multiple of the signal intensity in the double-band region from the signal intensity in the single-bond region. The difference is given by the *n*-hexane intensity. The exact factor (multiple) depends on the relative concentrations of 1- and 2-hexene, which can be obtained by evaluating the intensities of the three signals in the double-bond region.

The comparison of the total intensities of the spectra 2c and 2d gives an information about the isomerization of the hexene molecules after keeping the sample for one hour at 373 K. We see an intensity loss and a corresponding polymerization of about 30% in spectrum 2d with respect to spectrum 2c.

We acquired similar spectra as in Fig. 2 for all prepared MAS samples. These spectra were used for proving the loading. It is true that volumetric loading, by choosing a selected pressure in the loading volume, guarantees the shift of a calibrated quantity of molecules from the loading volume into the sample volume which is cooled with liquid nitrogen, as soon as the pressure in the vacuum line goes to less than 1% of the selected pressure. However, the final and most risky step of sample preparation is the sealing of the glass tube in a distance of about 3 mm to the zeolite bed. Insufficient cooling and slow sealing tend to reduce the concentration of the molecules in the sample, see Chapt. 2 in Supplementary Material. The spectroscopically confirmed, true values of loading were thus found to cover the whole range from zero loading (occurring under insufficient cooling and/or too slow sealing) up to the intended guest concentrations chosen to be one and 0.25 molecules

per crossing, respectively. The best loaded sample of *n*-butane with one molecule per crossing has been used as a reference sample for the ^{1}H MAS NMR intensity measurements of all sealed MAS samples. We denote the concentration of the loaded molecules by *L*. The unit of *L* is "mole of adsorbed molecules per mole of crossings". $L = 1$ corresponds to one molecule per crossing (or per channel intersection, or per 24 Si atoms or per ¼ unit cell). The samples used for the present study had loadings between $L = 0.1$ and 1. For simplicity, we use *L* without mentioning the unit.

The concentration dependence of the self-diffusion coefficient is not the main topic of the present investigation but, as a matter of course, influences our results. Caro et al. [1] reported about an increase of the self-diffusion coefficient of propane in silicalite-1 at 300 K by a factor of 100, if the loading is decreased from $L = 3.3$ to 0.5 molecules per crossing. Krishna and van Baten [18] calculated self-diffusivities, *D*, at 300 K in dependence on the loading *q* with the unit mol kg^{-1}. Using 1.442 kg as the molecular weight of one mole crossings in silicalite-1, we have $q = L/1.442$. The concentration dependences of the ethane and propane diffusivities in Fig. 4c of [18] can be described in the region $0.1 < L < 1$ by the slope $\mathrm{d}\lg D/\mathrm{d}\,L \approx -0.27$. We determined values $\Delta\lg D/\Delta L$ from our measurements by means of two different loadings ($0.1 < L < 1$) of ethane, ethene, propane, propene, *n*-butane, *n*-butene and obtained the values −0.66, −0.62, −0.58, −0.45, −0.62, and −0.49, respectively. In average, the concentration dependence observed in the present measurements follows the relation $\mathrm{d}\lg D/\mathrm{d}\,L = -0.55 \pm 0.10$. This means that, in the considered range of concentrations, an increase in loading by $\Delta L = 0.5$ leads to a decrease in *D* by 53%. We note that, as a matter of course, the diffusivities shown in Fig. 4 (with loadings $0.2 < L < 1.2$) will thus be stronger affected by this concentration dependence than those in Fig. 5 (with $0.1 < L < 0.3$).

Fig. 3 shows signal decays for the silicalite-1 sample loaded with one -propane molecule per crossing and measured at the temperature of 313 K. The observation time Δ, is increased in steps of a factor of two from 10 ms up to 160 ms. The gradient pulse length, δ, as the second parameter, is decreased in steps of a factor of $\sqrt{2}$ from 2 ms down to 0.5 ms. Thus, the product $\delta^2(\Delta - \delta/3) = 40\ \mathrm{ms}^3$ is constant for the five curves. The gradient, *g*, is varied as usual between 2% and 90% of its maximum intensity.

We will now demonstrate the conformity between the primary results of our measurements as exemplified by Fig. 3 and the formalism as presented by Eqs. (5) and (6), and illustrate the way how the intracrystalline diffusivities summarized in Figs. 4–6 have been determined from the primary data. Let us begin with

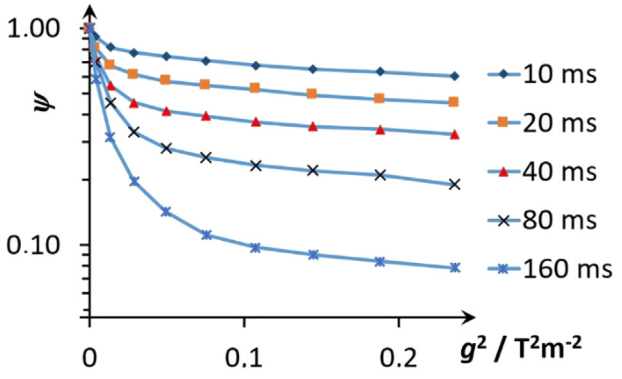

Fig. 3. Signal decays in dependence on the applied gradient intensities for the silicalite-1 sample loaded with propane ($L = 1$) and measured at 313 K. Observation times, Δ, are given in the figure and the product $\delta^2(\Delta - \delta/3) = 40\ \mathrm{ms}^3$ is constant for the five curves.

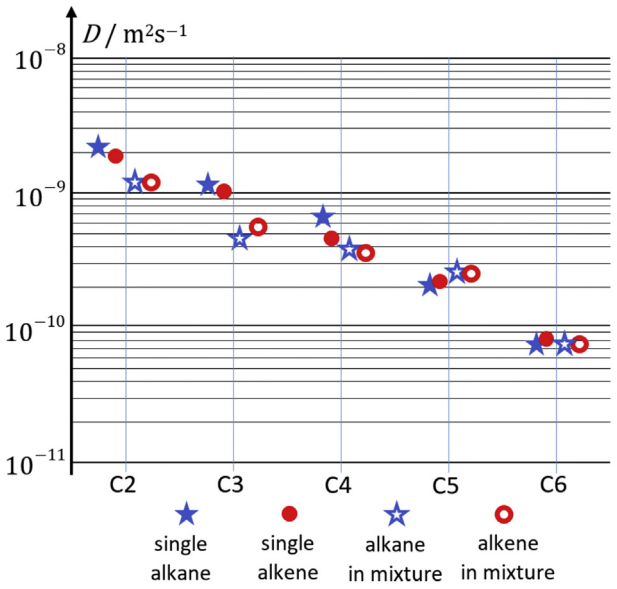

Fig. 4. Self-diffusion coefficients of *n*-alkanes, *n*-alkenes and *n*-alkane/*n*-alkene mixtures in silicalite-1 at 313 K for $0.2 < L < 1.2$.

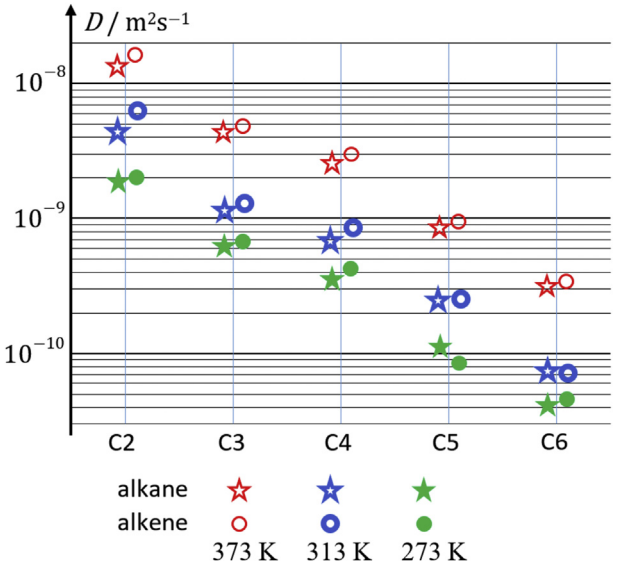

Fig. 5. Self-diffusion coefficients of *n*-alkanes and *n*-alkenes in silicalite-1 at 373 K, 313 K and 273 K for $0.1 < L < 0.3$.

recognizing two main features of the large-gradient asymptotes of the attenuation curves (Eq. (6)) in the logarithmic representation of the PFG NMR signal attenuations shown in Fig. 3., namely (i) a set of close to parallel straight lines corresponding to the second term on the right-hand side of Eq. (6), and (ii) the shift of these lines towards decreasing values of ψ with increasing observation time Δ as a consequence of the first term on the right-hand side of eq. (6). Extrapolation of this part of the signal attenuation for $\Delta = 160$ ms, e.g., towards the ordinate yields a value of 0.117 at the intersection. This value indicates the fraction of guest molecules which, during the chosen diffusion time, have not left their crystallites. With Eq. (6) (i.e. by setting $g = 0$ and considering $\ln 0.117 = -160\ \mathrm{ms}/\tau_{\mathrm{intra}}$) this value may immediately be transferred into an intracrystalline mean life time of $\tau_{\mathrm{intra}} = 75$ ms.

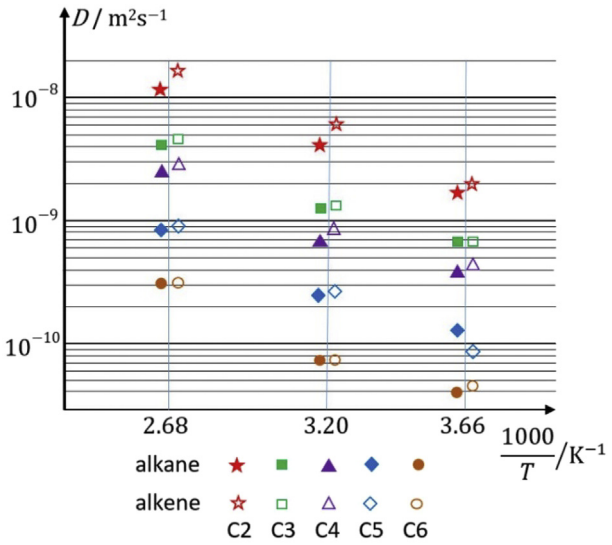

Fig. 6. Arrhenius plot of the self-diffusion coefficients of *n*-alkanes and *n*-alkenes in silicalite-1.

Measurement with the largest observation times offer the best options for measuring the long-range diffusivities since they give rise to the most pronounced first decay in the signal attenuation curve. In the given case, this first steep decay yields a long-range diffusivity of 2×10^{-8} m^{2}s^{-1}.

The measurement of intracrystalline diffusion, however, necessitates measurement with the smallest possible observation time for reducing the impediment by confinement (anticorrelations of subsequent displacements) by the crystallite boundaries [16,17]. In the example given by Fig. 3, best conditions for the measurement of genuine intracrystalline diffusion are provided with the shortest observation time of $\Delta = 10$ ms. By, once again, extrapolating the second branch in the attenuation curve to the ordinate, 80% of the guest molecules are found to remain within their crystallites during the observation time. The slope of the second branch yields a value of 2.28×10^{-10} m^{2}s^{-1} for the intracrystalline diffusivity. It is this second part of the signal attenuation curve which, throughout this paper, has been used for the determination of the intracrystalline diffusivities.

Before presenting and discussing these results in more detail we provide two consistency checks of the thus determined diffusivity data. The root-mean-square displacement $\sqrt{l^2}$ obtained with the resulting diffusivity of 2.28×10^{-10} m^{2}s^{-1} and the observation time of 10 ms via Eq. (2) yields a value of 3.7 μm. With the range of crystal sizes ((20–40) μm × (25–50) μm × (100–200) μm, see Fig. 1) given above, this result is in nice correspondence with the implication that only a minor part of the guest molecules will be notably affected by confinement effects due to the external crystallite surface. We may, further on, use the data obtained for the intracrystalline diffusivity (2.28×10^{-10} m^{2}s^{-1}) and the intracrystralline mean life time (τ_{intra}= 75 ms) for an estimate of the crystal size dimensions relevant for mass exchange. By neglecting possible influences of surface barriers, see Ref. [19], such an approach may be based on using the relations for the so-called first statistical moments [20] as an estimate of the intracrystalline mean life time. For a cylinder with an axis notably exceeding its diameter d (which, for the given purpose, serves as a reasonable approach of the crystal shape, see Fig. 1), one has $\tau_{intra} = d^2/(32D)$. With the above given values of diffusivity and intracrystalline mean live time one thus obtains a value of $d = 23$ which is indeed within the range of crystal dimensions as appearing by microscopic inspection.

4. Results and discussion

The total loading $L = 1$ was the target of the sample preparation for the investigation of the mixture diffusion. But an exact loading could not be realized due to the difficult sealing procedure. Fig. 4 presents the self-diffusion coefficients for the single components and the mixtures at the temperature of 313 K. The experimental error of the values is about the size of the symbols in the figure. The *L*-values of the included samples are, in the order *n*-alkane, *n*-alkene and *n*-alkane/*n*-alkene mixtures, for C2 0.6, 0.6 and 0.5/0.4, for C3 0.9, 0.9 and 0.7/0.5, for C4 0.3, 0.7 and 0.6/0.2, for C5 0.2, 0.4 and 0.3/0.1, for C6 0.6, 0.5 and 0.3/0.1, respectively.

The above discussed loading dependence influences the results. Nevertheless, we can conclude that, neither for the comparison of mixture components with single components nor for the comparison between *n*-alkanes and *n*-alkenes, these differences are of any major relevance. The diffusivity data offer rather a clearly perceptible trend.

This visual conclusion can be quantitatively supported in the following way: We use the diffusivities at 313 K, which are presented in Fig. 4, and in addition, the results of similar measurements of the identical samples at 273 K and 373 K. Then we calculate the mean value and standard deviation of the 15 ratios D_{alkane}/D_{alkene} for all mixture measurements. The result is $D_{alkane}/D_{alkene} = 1.01 \pm 0.25$. The different sample loadings do not influence this consideration for the mixture samples.

But the comparison between the single components and the two mixture components is more complicated, because the different loadings of the samples must be taken into account. First, we calculate so-called “zero-loading” self-diffusion coefficients D_0 via the relation $\lg D_0 = \lg D + 0.55\, L$ for all measurements. Next, we compute from the four components (single *n*-alkane, single *n*-alkene, *n*-alkane in mixture and *n*-alkene in mixture) at each temperature and carbon number (chain length) a mean value and four relative values. Finally, we calculate from 15 relative values (5 carbon numbers at 3 temperatures) a mean value and standard deviation for each component. It results 0.87 ± 0.25, 1.10 ± 0.34, 0.90 ± 0.15 and 0.89 ± 0.23 for single *n*-alkane, single *n*-alkene, *n*-alkane in mixture and *n*-alkene in mixture, respectively. The value 1.00 is always included in the limits of the standard deviation.

The total loading $L = 1/4$ was the target of the sample preparation for a comparison of different carbon numbers and different measuring temperatures. Fig. 5 presents the self-diffusion coefficients for the *n*-alkanes and *n*-alkenes. The *L*-values of the included *n*-alkane and *n*-alkene samples are for C2: 0.2 and 0.2, for C3: 0.1 and 0.2, for C4: 0.2 and 0.1, for C5: 0.2 and 0.3, for C6: 0.2 and 0.2, respectively. Once again, also for the smaller loadings only small differences between the diffusivities of *n*-alkanes and *n*-alkenes are observed. The half-logarithmic presentation of the values in Fig. 5 shows that lg *D* can be approximated by a linear dependence on the carbon number, *C*. The increase of *C* by one step in the line C2, C3, C4, C5, C6 causes a decrease of the self-diffusion coefficient by a factor of about 0.4.

Fig. 6 presents an Arrhenius plot of the diffusivity data shown in Fig. 5. A significant change of the slope cannot be observed, if we use the two pairs 278 K/313K and 313 K/373 K. Therefore, we use only the values for 278 K and 378 K for the determination of an apparent activation energy. We obtained the values 16.6, 18.2, 16.2, 17.2, 16.9, 16.6, 17.0, 20.5, 17.3 and 16.9 kJ mol^{-1} for ethane, ethene, propane, propene, *n*-butane, *n*-butene, *n*-pentane, *n*-pentene, *n*-

hexane and *n*-hexene, respectively. Most values are in the range 18 ± 2 kJ mol^{-1}.

This finding represents a remarkable difference to the trend in the activation energies of the self-diffusivities of *n*-alkanes in zeolite NaX [21] and NaCaA [22] where logarithmic chain length dependencies of guest diffusivities have already been considered. In the latter case, i.e. for NaCaA, the series of homologues is started with propane for avoiding the additional influence of variation in the critical diameter which, for the narrow-pore zeolites NaCaA are known to be of large influence [23]. But the most important reference for the present study is a chain length dependency of the PFG NMR diffusivity of *n*-alkanes in MFI-type zeolites in the range from C2 to C12 by Jobic et al. [24]. Their loading corresponds to six carbon atoms per channel intersection [24], and the self-diffusion coefficients show a monotonous decrease by a factor of about 0.54 per carbon atom number in the whole range of *C*. The step from C6 to C7 is important for our discussion. Therefore, we performed an additional MAS PFG NMR experiment and obtained for *n*-heptane, with $L = 0.15$, at 313 K, a value of $D = 4.2 \times 10^{-11}$ m^{2}s^{-1}. The comparison with the corresponding value for *n*-hexane at 313 K, $D = 7.7 \times 10^{-11}$ m^{2}s^{-1}, gives a decrease by the factor of 0.55. Concluding we can state that PFG NMR monitors, in dependence on the *C* number, a logarithmic linear decrease of the *n*-alkane diffusivity in the range from C2 to C12. MAS PFG NMR has shown that it holds also for alkenes in the monitored range from C2 to C6.

A different chain length behavior, especially around C6, was obtained by a hierarchical simulation approach [25]. There are small and subtle differences in the bond lengths and bond angles of ethene/ethane, propene/propane; see Supplementary Material Fig. S10. Such differences are not of significant importance for diffusion in the 0.55 nm channels of MFI zeolite. Consequently, the diffusivities in MFI zeolites were calculated only for n-alkanes. Supplementary Material Fig. S11 summarizes MD data on diffusivity of n-alkanes, culled from the literature [4,18,26,27], for comparison with MAS PFG and PFG NMR data. The MD data are significantly higher in magnitude; this is to be expected because the simulations are sensitive to the choice of the force fields used in the simulations, as has been demonstrated by Krishna and van Baten [26].

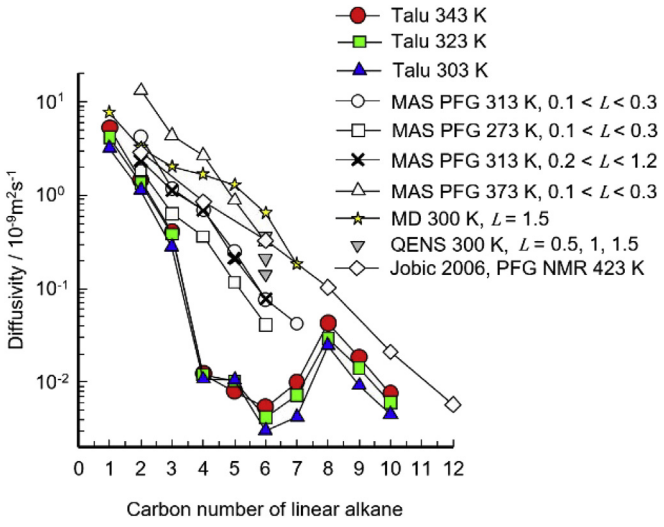

Fig. 7. Comparison of experimental data (MAS PFG NMR (this study), PFG NMR [24] and QENS [24,32], with membrane permeation data of Talu et al. [28] (the data are culled from Table 2 of their paper).

Fig. 7 compares experimental diffusivity data (MAS PFG NMR, PFG NMR and QENS), with the data of Talu et al. [28] that are determined from membrane permeation experiments (the data are culled from Table 2 of their paper). The Talu data are not at constant loading; the loadings increase with increasing chain length because of stronger adsorption. There is a sharp minimum in the diffusivity data for *n*-hexane. This minimum is also found for the MD simulated diffusivities at "zero-loading".

There is indeed a fundamental explanation for the possibility of the occurrence of a minimum in the zero-loading diffusivity for *n*-hexane. While the length of an *n*-hexane molecule is commensurate with the distance between the intersections of MFI zeolite (cf. snapshot in SM Fig. S12a) an *n*-heptane molecule is slightly longer than the distance between channel intersections (see SM Fig. S12b). From these differences in molecular lengths of *n*-hexane (commensurate) and *n*-heptane (incommensurate) one may in fact expect an influence on the diffusion characteristics, tending to an enhancement in diffusivity under the conditions of incommensurability, see Ref. [29].

However, with the present data, the occurrence of such a diffusivity increase due to incommensurability for *n*-heptane in MFI cannot be confirmed in the range of the considered loadings. This is in accordance with also previous investigations as summarized in Fig. 7 which shows the MD data of Krishna and van Baten for self-diffusivity at loading $L = 1.5$ and previous PFG NMR data. All these diffusivity data show a monotonic decrease with increasing *C* numbers, in line with also the results of the present MAS PFG NMR studies.

Self-diffusion coefficients of *n*-alkanes in silicalite-1 were repeatedly measured by PFG NMR [1,24,30], whereas corresponding studies on *n*-alkenes are rather rare. Caro et al. [1] measured for one molecule per crossing ($L = 1$) at 300 K a self-diffusion coefficients of about 6×10^{-9} m^{2}s^{-1} for ethane and 4×10^{-9} m^{2}s^{-1} for propane. Jobic et al. [24] measured at 298 K values of about 6×10^{-10} m^{2}s^{-1} for *n*-butane ($L = 1{,}5$) and 1.3×10^{-10} m^{2}s^{-1} for *n*-hexane ($L = 1$). Fig. 4 shows that our self-diffusion coefficients of *n*-alkanes lie in the same range. The root-mean-square displacement covered by the molecules s in our measurements is in the range between 4 and 15 μm and, thus, smaller than the size of the silicalite-1 crystallites. We were unable to observe intracrystalline transport barriers, which Vasenkov et al. [30] were able to detect with displacements over a further reduced range, between 1 and 4 μm. The existence of such transport barriers (which remain out of the reach of our measurements) could be the reason that our self-diffusion coefficients for ethane and propane in case of low loadings at 313 K, see Fig. 5, are by a factor of 2–3 smaller than the values which were calculated by Krishna and van Baten [18] for a barrier-free silicalite-1 at 300 K. It could also explain that we obtained a loading dependence of the self-diffusion coefficient of $\frac{d\lg D}{d\,L} = -0.55$ in the range $0.1 < L < 1$, whereas the value $\frac{d\lg D}{d\,L} = -0.28$ can be derived from the calculations by Krishna and van Baten [18].

We found in the literature only one PFG NMR investigation of *n*-alkenes adsorbed in silicalite-1: Snurr et al. [31] measured the self-diffusion of ethene in silicalite-1 ($L = 3$) in the temperature range from 200 K to 300 K and obtained $D = 8.2 \times 10^{-10}$ m^{2}s^{-1} for 300 K and a slope of the Arrhenius plot corresponding to $E = 5.2$ kJ mol^{-1}. We measured, at 313 K and a significantly lower loading ($L = 0.6$), a 2.4 times higher *D* value. The present investigation is, to our best knowledge, the first systematic PFG NMR study of the *n*-alkene self-diffusion in silicalite-1.

5. Conclusions

The main result of the present study is not surprising: *n*-alkanes and *n*-alkenes have the same diffusivity in silicalite-1. This holds for the single components and the *n*-alkane/*n*-alkene mixtures. The result was expected but never proven before. Most astonishingly, however, and deviating from the behavior observed with zeolites NaX and NaCaA, there was, for all guest molecules considered (*n*-alkanes and *n*-alkenes with $2 \leq n \leq 6$), no significant variation in the activation energy of self-diffusion as appearing from the slope of the Arrhenius plots. Notably for the small loadings ($0.1 < L < 0.3$) all activation energies were found to lie in the range 18 ± 2 kJ mol^{-1}.

Acknowledgement

This work was supported by the Deutsche Forschungsgemeinschaft (grants HA 1893/16 and Avance 750) and for A.S. by the Russian Academy of Sciences (grant 0303-2016-0003).

Appendix A. Supplementary data

Supplementary data related to this article can be found at http://dx.doi.org/10.1016/j.micromeso.2017.08.015.

References

[1] J. Caro, M. Bülow, W. Schirmer, J. Kärger, W. Heink, H. Pfeifer, S.P. Zdanov, J. Chem. Soc. Faraday Trans. I (81) (1985) 2541–2550.
[2] H. Jobic, D.N. Theodorou, Microporous Mesoporous Mater 102 (2007) 21–50.
[3] R. Krishna, J.M. van Baten, J. Phys. Chem. B 109 (2005) 6386–6396.
[4] R. Krishna, Microporous Mesoporous Mater 185 (2014) 30–50.
[5] R. Krishna, Phys. Chem. Chem. Phys. 18 (2016) 15482–15495.
[6] U. Böhme, B. Barth, C. Paula, A. Kuhnt, W. Schwieger, A. Mundstock, J. Caro, M. Hartmann, Langmuir 29 (2013) 8592–8600.
[7] C. Chmelik, D. Freude, H. Bux, J. Haase, Microporous Mesoporous Mater 147 (2012) 135–141.
[8] P. Rousselot-Pailley, D. Maux, J.M. Wieruszeski, J.L. Aubagnac, J. Martinez, G. Lippens, Tetrahedron 56 (2000) 5163–5167.
[9] H. Schröder, J. Comb. Chem. 6 (2003) 741–753.
[10] H.C. Gaede, K. Gawrisch, Magn. Reson. Chem. 42 (2004) 115–122.
[11] A. Pampel, K. Zick, H. Glauner, F. Engelke, J. Am. Chem. Soc. 126 (2004) 9534–9535.
[12] M. Fernandez, J. Kärger, D. Freude, A. Pampel, J.M. van Baten, R. Krishna, Microporous Mesoporous Mater 105 (2007) 124–131.
[13] T. Mildner, H. Ernst, D. Freude, Solid State Nucl. Magn. Reson 5 (1995) 169–271.
[14] M. Holz, S.R. Heil, A. Sacco, Phys. Chem. Chem. Phys. 2 (2000) 4740–4742.
[15] J. Kärger, D.M. Ruthven, D.N. Theodorou, Diffusion in Nanoporous Materials, Wiley-VCH, Weinheim, 2012.
[16] J. Kärger, M. Kocirik, A. Zikanova, J. Colloid Interface Sci. 84 (1981) 240–249.
[17] P. Zeigermann, S. Naumov, S. Mascotto, J. Kärger, B.M. Smarsly, R. Valiullin, Langmuir 28 (2012) 3621–3632.
[18] R. Krishna, J.M. van Baten, Chem. Eng. Technol. 30 (2007) 1235–1241.
[19] D. Tzoulaki, L. Heinke, W. Schmidt, U. Wilczok, J. Kärger, Angew. Chem. Int. Ed. 47 (2008) 3954–3957.
[20] R.M. Barrer, Zeolites and Clay Minerals as Sorbents and Molecular Sieves, Academic Press, London, 1978.
[21] J. Kärger, H. Pfeifer, M. Rauscher, A. Walter, J. Chem. Soc. Faraday Trans. I (76) (1980) 717–737.
[22] W. Heink, J. Kärger, H. Pfeifer, K.P. Datema, A.K. Nowak, J. Chem. Soc. Faraday Trans. I (88) (1992) 3505–3509.
[23] D.M. Ruthven, Microporous Mesoporous Mater 162 (2012) 69–79.
[24] H. Jobic, W. Schmidt, C.B. Krause, J. Kärger, Microporous Mesoporous Mater 90 (2006) 299–306.
[25] E.J. Maginn, A.T. Bell, D.N. Theodorou, J. Phys. Chem. A 100 (1996) 7155–7173.
[26] R. Krishna, J.M. van Baten, Microporous Mesoporous Mater 109 (2008) 91–108.
[27] R. Krishna, J.M. van Baten, Microporous Mesoporous Mater 107 (2008) 296–298.
[28] O. Talu, M.S. Sun, D.B. Shah, A.I.Ch.E.J. 44 (1998) 681–694.
[29] H. Wu, Q. Gong, D.H. Olson, J. Li, Chem. Rev. 112 (2012) 836–868.
[30] S. Vasenkov, W. Böhlmann, P. Galvosas, O. Geier, H. Liu, J. Kärger, J. Phys. Chem. B 105 (2001) 5922–5927.
[31] R.Q. Snurr, A. Hagen, H. Ernst, H.B. Schwarz, S. Ernst, J. Weitkamp, J. Kärger, J. Catal. 163 (1996) 130–137.
[32] H. Jobic, N. Laloue, C. Laroche, J.M. van Baten, R. Krishna, J. Phys. Chem. B 110 (2006) 2195–2201.

Alkane/alkene mixture diffusion in silicalite-1 studied by MAS PFG NMR

Nina Dvoyaskina,[a] Dieter Freude,*[a] Alexander G. Stepanov,[b c] Winfried Böhlmann,[a] Rajamani Krishna[d], Jörg Kärger[a], Jürgen Haase[a]

[a] Faculty for Physics and Earth Sciences, Leipzig University, Linnéstr. 5, 04103 Leipzig, Germany

[b] Boreskov Institute of Catalysis, Siberian Branch of Russian Academy of Sciences, Prospekt Akademika Lavrentieva 5, Novosibirsk, 630090, Russia

[c] Novosibirsk State University, Pirogova Str. 2, Novosibirsk 630090, Russia

[d] Van't Hoff Institute for Molecular Sciences, University of Amsterdam, Science Park 904, 1098 XH Amsterdam, The Netherlands

* Corresponding author, E-mail: freude@uni-leipzig.de

Supplementary material

1. Silicalite-1, after synthesis treatment

An ideal silicalite-1 should not catalyze reactions of adsorbed molecules. However, all real silicalites-1 possess, after the removal of the template, a small concentration of silanol groups, which are localized in framework defects and on the outer surface. These groups react as weak acids and are able to polymerize alkene molecules.

We measured the ^{1}H MAS NMR intensity of a sealed glass tube containing silicalite-1 after activation at 673 K. In addition, we measured the signal intensity of an empty glass tube in the rotor and the empty MAS rotor without any sample. Both, the empty MAS rotor and the glass tube show a weak signal of silanol groups. The comparison of the intensities showed that the silanol intensity of the sealed silicalite-1 is not significantly different from the signal of the empty glass tube. Then the sealed silicalite-1 sample without adsorbed molecules and a sample of known ethane loading were measured, and an upper limit for the silanol concentration of the activated silicalite-1 of 0.2 OH groups per unit cell was estimated.

The activated silicalite-1 catalyzes the polymerization of adsorbed n-alkene molecules at ambient temperature as we could observe by the decrease of the ^{1}H MAS NMR alkene signal some days after the loading of the as-synthesized and activated silicalite-1. The polymerization took place within a few minutes at a temperature of 373 K. The polymer consisting of methylene groups gives a 30 kHz broad NMR signal, whereas the resolved ^{1}H MAS NMR peaks of adsorbed molecules have a *fwhm* (full with at half maximum) in the order of magnitude of 100 Hz.

The catalytic activity of the zeolite was decreased by a hydrothermal healing procedure. The right-hand side of the glass device (outer diameter 13 mm, see Fig. S1) was filled with the calcined silicalite-1. A ring oven covered the part of the device up to the second capillary. The upright part of the device contained water. It was located outside the oven, and the water

temperature was about 303 K whereas the temperature of the oven and the zeolite was 673 K. The hydrothermal treatment at 30 mbar water pressure took one week.

Fig. S1. Glass device for the hydrothermal healing procedure of the zeolite at 400 °C and 30 mbar water pressure.

After the healing procedure, the alkene loaded samples showed in the ^{1}H MAS NMR experiments that the alkene polymerization is not significant at 313 K and causes 20% ethene loss and 30% *n*-hexene loss during a one-hour lasting experiment at 373 K. Imperatively, all samples were kept in a cooler at 255 K between loading and measurement.

The size of the silicalite-1 crystallites varies in the range (20−40) µm × (25−50) µm × (100−200) µm (see Fig. 2). Fig. S2 shows the ^{29}Si MAS NMR spectra of the slightly hydrated samples before and after hydrothermal healing. The spectra were measured at a resonance frequency of 149 MHz using a rotation frequency of 10 kHz and an acquisition time of 1d. The room temperature spectrum of a siliceous MFI type zeolite consists of 24 signals of identical intensity due to the 24 silicon sites [1]. Only one line of our spectra at −110 ppm is well resolved and has an intensity of 1/24 of the total intensity of the spectrum and an *fwhm* of about 70 Hz. We conclude from the almost identical spectra that the hydrothermal healing procedure influences neither the near-range order nor structure defects, which influence the *fwhm* of the single lines [1].

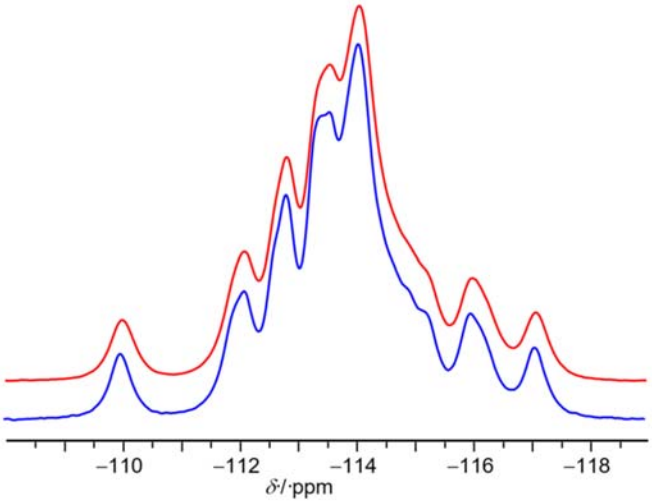

Fig. S2. ^{29}Si MAS NMR spectra of the as-synthesized silicalite-1 after calcination (upper red spectrum) and the hydrothermally healed silicalite-1 (lower blue spectrum).

2. MAS sample preparation

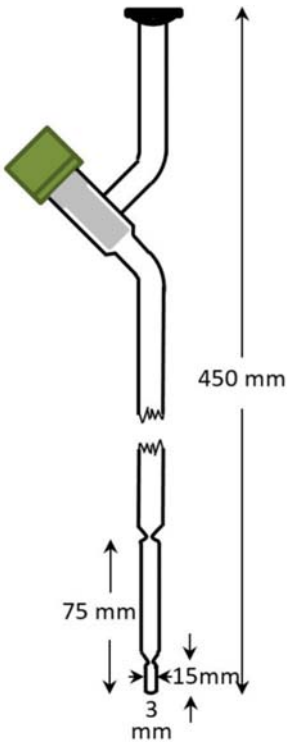

Figure S3. Activation and loading device.

The silicalite-1 contains less than 1 wt.% water after the healing procedure. The samples for the NMR measurements were outgassed (activated) by heating 25 mg of the zeolite sample in a glass tube of 3 mm outer diameter and a distance of 15 mm between bottom and first capillary of the glass tube (see Fig. S3). The tube was introduced 200 mm deep into an oven and connected to the vacuum line. The valve was slowly opened. The temperature was increased using a rate of 50 K h^{-1} up to 673 K and remained at this value for 48 h with a vacuum of about 10^{-2} Pa. After cooling down to room temperature, the samples were loaded by means of a chosen gas pressure in a calibrated loading volume. During the loading process the sample tube was cooled with liquid nitrogen to ensure that the gas completely adsorbed into the pores of the silicalite. Thereafter, the loaded samples were sealed in two steps. The bottom of the device was put into another vessel with liquid nitrogen which is 10 mm deep (see Fig. S4). The first sealing took place after one minute at the second capillary. The lower residual part, 75 mm high, was put again 10 mm deep into liquid nitrogen. After another two minutes, the part was mounted into the glass sealing holder (see Fig. S5). The holder consists of a brass head and a vinyl tube. It was cooled for 2 minutes in liquid nitrogen before each use. Finally, the sample was quickly and symmetrically fused at the first capillary.

Fig. S4. Cooling device, which can be filled with liquid nitrogen. The glass tubes are placed into the inner hole. The outer holes are deeper and used for an additional cooling of the device.

Figure S5. Glass sealing holder consisting of a brass head and a vinyl tube.

3. NMR signal separation

Hesse *et al.* [2] present values of the chemical shifts of ^{1}H nuclei of alkane and alkene molecules. According to their data methyl groups of *n*-alkanes show ^{1}H NMR signals in the range of 0.86 ppm to 0.91 ppm and the methylene groups between 1.23 ppm and 1.33 ppm. The ^{1}H nuclei of *n*-alkenes connected to double bonded carbon atoms have chemical shifts of 4.85 ppm to 5.81 ppm. Methylene groups in neighborhood to a double bonded carbon pair show a signal at about 2 ppm.

Chemical shift data of single molecules [2] are shifts of molecules in solution of $CDCl_3$ or CCl_4. Adsorbed molecules interact with the host framework causing a chemical shift with respect to isolated molecules. Relatively small differences occur for the ion-free zeolite silicalite-1. We observed adsorption shifts in the range of 0.01 ppm (C_2H_5) to 0.1 ppm (terminal CH_2 of 1-butene).

In addition, the susceptibility of the porous zeolites contributes to a resonance shift of the intracrystalline adsorbed molecules and a different shift of the non-adsorbed molecules in the intercrystalline space. Fig. S6 shows relatively weak and narrow signals of gaseous ethene and ethane shifted to higher field of about 0.25 ppm compared with strong signals of adsorbed ethene (about 5.5 ppm) and ethane (about 1 ppm) in the silicalite-1 at a temperature of 373 K. Similar spectra are observed at room temperature at higher loading.

Non-adsorbed molecules in the gas phase have a very high self-diffusivity. Their signals disappear already for the smallest gradient in our MAS PFG NMR spectra. Measurements of the gas phase signal decay upon very weak gradient strengths gave a self-diffusion coefficient of $D = 1.6 \times 10^{-5}$ m^2 s^{-1} for ethane and ethene gas phase diffusivities at 303 K in a ZIF-8 sample [3].

The resonance shift of gaseous molecules is a possible internal reference for the chemical shift. However, the zeolitic environment causes a susceptibility shift of the gaseous molecules. Therefore, a rotor filled with polydimethylsiloxane (PDMS, 0.07 ppm with respect to tetramethylsilane, TMS) is used as external reference.

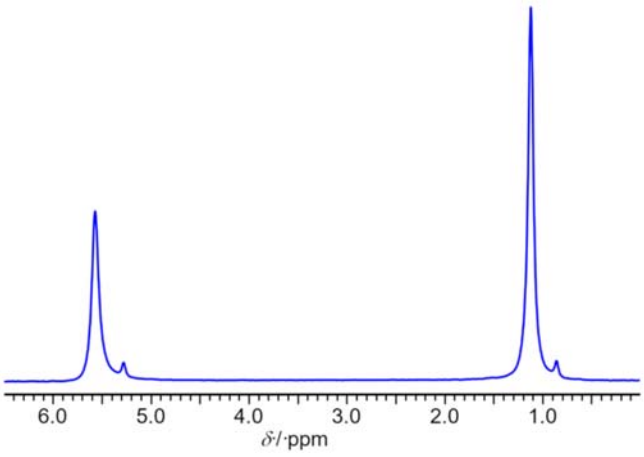

Fig. S6. ^{1}H MAS NMR Signals of an ethene/ethane mixture in silicalite-1 at T = 373 K.

The determination of the correspondent self-diffusion coefficients requires an integration of the separated peak intensities due to *n*-alkanes and *n*-alkenes. This is relatively easy and still possible up to three carbon atoms and for mixtures with 2-butene. Studying 1-butene and longer chain molecules, the separation can be performed by dividing the spectral range into two parts. The low field region between 3 to 8 ppm contains signals of hydrogen atoms connected to double bonded carbon atoms. The high field region between −1 to 3 ppm consists of a superposition of alkane and alkene signals. The alkene intensity in the high field region is a multiple, *f*, of their intensity in the low field region. The factors are *f* = 5/3 for 1-butene, 6/2 for 2-butene, 7/3 for 1-pentene, 8/2 for 2-pentene, 9/3 for 1-hexene, 10/2 for 2- or 3-hexene, 13/3 for 1-octene, 14/2 for 2-, 3- or 4-octene, 17/3 for 1-decene, and 18/2 for 2-, 3- or 4-decene.

4. Double bond shift

We used 1-alkenes or 2-alkenes for the loading. But a mixture of 1-alkenes and alkenes with other double bond positions occurs in our sample, since a double bond shift takes place. The relative concentrations are $x_1 + x_{other} = 1$ and can be determined by ^{1}H MAS NMR intensity measurements. We use $f = x_1 f_1 + x_{other} f_{other}$ instead of the single factors, *f*, given above.

Silicalite-1 behaves as a weak catalyst and causes a double bond shift of the adsorbed *n*-butene [4] and larger alkenes. Two samples were prepared using 1-butene and 2-butene, respectively, to study the behavior of the adsorbed molecules. The samples were treated at 373 K for one hour resulting in the same equilibrium concentration of both samples about 9% 1-butene and 91% 2-butene. This agrees well with the equilibrium constant of 11.66 given by Meyer [4].

5. Extended presentation of the PFG NMR method

PFG NMR diffusion measurements are performed on a radio frequency (RF) pulse sequence combined with a gradient pulse sequence. The Hahn echo sequence (π/2 and π pulse) and the stimulated echo sequence (three π/2 pulses) generate spin echoes. Gradient pulses start after the first and after the last RF pulse with a duration δ and a maximum intensity g. One obtains an integral of $\delta \times g$ for a rectangular gradient pulse shape. A sinusoidal pulse shape like in Fig. S7 is preferred, in order to facilitate the switching of the strong gradient currents. The integral equals to $\delta \times g \times 2/\pi$ for a sine-shaped pulse. Alternating gradient pulse pairs (with a RF π pulse in between) average out the influence of the local field gradients of the material under study and reduce the influence of eddy currents as well. The integral of a sine-shaped pulse pair is $\delta \times g \times 4/\pi$.

Tanner [5] introduced the stimulated echo procedure for PFG NMR experiments. Cotts *et al.* [6] applied alternating gradient pulses. Wu et al. [7] added the eddy current delay by means of two additional π/2 pulses and observed the free induction after the last pulse instead of the stimulated echo. A variation of this pulse sequence by application of sine-shaped gradient pulses is shown in Fig. S7. The sequence for alternating sine shaped gradient pulses and longitudinal eddy current delay (LED) consists of seven RF pulses, two alternating magnetic field gradient pulse pairs (the duration for a single pulse is δ and the intensity is g) and two eddy current quench pulses. The latter destroy undesired coherences in the time interval between

two adjacent π/2 pulses, when the magnetization points into the z-direction. The observation time of the diffusion, Δ, is the time span between the starts of the two gradient pairs. The eddy current delay, τ_{ecd}, is 5 ms.

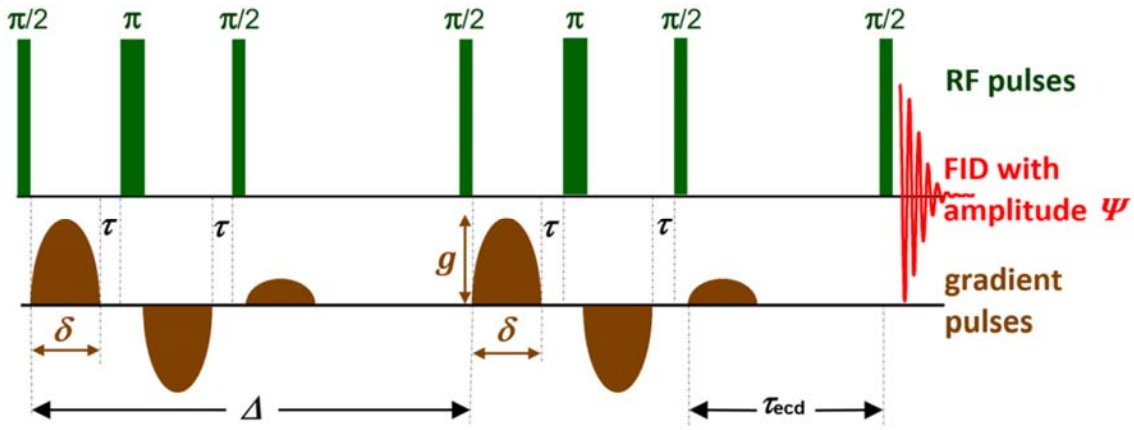

Fig. S7. Stimulated spin-echo sequence with eddy current delay, two sine-shaped bipolar gradient pulse pairs and two gradient quench pulses, after Fig. 2 in [8].

The delay τ, between gradient and RF pulses is necessary, because the ring down of the gradient current immediately after the gradient pulse is harmful for the selectivity of the next RF pulse. We used $\tau \approx 0.5$ ms. The eddy current delay, τ_{ecd}, overcomes the problem that the NMR signal is strongly distorted by a directly preceding gradient pulse. We used $\tau_{ecd} \approx 4.5$ ms. A repetition delay of 5 s is used, in order to avoid a heading of the gradient coils. It is commonly much longer than the fivefold of the longitudinal relaxation time T_1. Gradient quench pulses have 15 % of the maximum intensity.

The self-diffusion coefficient, D, of molecules is obtained from the decay of the amplitude, S, of the FID in dependence on the squared field gradient intensity, g^2, by the equation

$$\psi(g^2) = \frac{S(g^2)}{S_0} = \exp\left[-D\left(\frac{4\delta g\gamma}{\pi}\right)^2\left(\Delta - \frac{\tau}{2} - \frac{2\delta}{3} - p_\pi\right)\right]. \qquad \text{(S1)}$$

S_0 denotes the value for a zero-gradient. The magnetogyric ratio, γ, amounts for ^{1}H nuclei $\gamma = 26.7522128 \times 10^7$ s^{-1}T^{-1}. The duration of a π pulse is denoted as p_π and amounts a few microseconds in dependence on the used probe. Eq. (1) describes the signal decay for single-component isotropic diffusion and is identical with Eq. (1) in [8]. Eq. (1) can be rewritten as

$$\ln\psi(g^2) = -D\left(\frac{4\delta g\gamma}{\pi}\right)^2\Delta' = -Ag^2. \qquad \text{(S2)}$$

The corrected observation time, Δ', corresponds to the right round bracket in Eq. (1). The slope of a linear fit of $\ln \psi(g^2)$ has a negative value $-A$ with the dimension $\mathrm{T^{-2}m^2}$. If we use only two points (X) and (Y) for the determination of the slope, we have

$$-A = \frac{\ln[\Psi(X)/\Psi(Y)]}{g^2(X) - g^2(Y)}. \tag{S3}$$

Using the magnetogyric ratio of γ= 26.7522128 × 10^7 $\mathrm{s^{-1}T^{-1}}$ for ^{1}H nuclei we obtain

$$D = \frac{-A}{\Delta'}\left(\frac{\pi}{4\delta\gamma}\right)^2 \approx \frac{-A}{\delta^2\Delta'} \times 8.619\times10^{-18}\times \mathrm{s^{-2}T^{-2}}. \tag{S4}$$

Eq. (4) can be rewritten, by using D in the unit of $\mathrm{m^2s^{-1}}$, the slope $-A$ in the unit of $\mathrm{T^{-2}m^2}$ and the unit ms instead of s for the values δ and Δ', in the form of a dimensionless equation:

$$\frac{D}{\mathrm{m^2s^{-1}}} \approx \frac{-A}{\mathrm{T^{-2}m^2}} \times \frac{\mathrm{ms}^3}{\delta^2\Delta'} \times 8.619\times10^{-9}. \tag{S5}$$

The signal function Ψ, which is used in Eqs. (1−3), denotes the maximum intensity of the relaxation function (echo or FID) in the time scale. However, it is common use to evaluate the integral of the signal in the frequency domain after the Fourier transform of the time domain. Both procedures are identical for single-component diffusion from a theoretical point of view. For mixture diffusion, the processing of signals requires the frequency domain. The Bruker processing program t1guide provides the one-step calculation for one or several signal areas.

We start our measurement commonly at 2% of the maximum gradient; the second point comes with 12%, if the range goes from 2% to 90%. The stimulated echo or the FID in Fig. S7 contains some undesired signal contributions, which are not fully averaged out by means of the 16-phase-cycle [8]. But these signal contributions, which still exist for the weak gradient of 2%, disappear under the influence of the stronger (12% or more) field gradients. Therefore, we must skip the first point, which corresponds to the 2%-gradient, for the evaluation of the signal decay under the influence of the gradient.

As mentioned above, Eq. (1) describes the isotropic one-component diffusion. The signal decay in dependence on the squared field gradient becomes more complicated for diffusion anisotropy. We expect isotropic diffusion in the FAU-type zeolites with cubic symmetry. The observation of the diffusion anisotropy and the different principal elements D_x, D_y and D_z of the diffusion tensor in the non-cubic MFI-type zeolites requires the monitoring of the attenuation by some orders of magnitude, as it was performed by Hong et al.[9]. This effect is not considered in the present study. However, a superposition of two exponential decays was observed in some cases, if the intracrystalline self-diffusion process was superimposed by an intercrystalline diffusion of the molecules.

Fig. S8 demonstrates that the decay of the signals of an ethane/ethene mixture is not mono-exponential at 313 K. The total loading is about one molecule per crossing. The signals at the left and right side correspond to ethane and ethane, respectively.

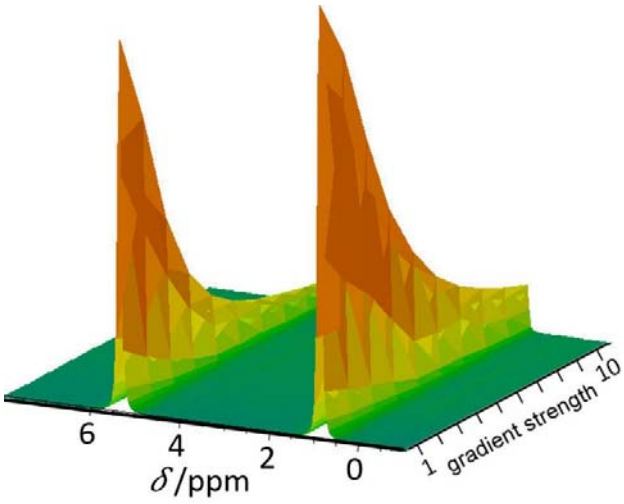

Fig. S8. 2D presentation of the signal decay with linearly increasing strength of the gradient pulses for a sample loaded with an ethane/ethane mixture and measured at 313 K.

Fig. S9 describes Eqs. (4−6). In addition to the part of the figure, which was taken from Ref. [10], we show for the special case $\tau_{\mathrm{intra}} = 2\Delta$ a biexponential fit of Eq. (5) in the initial region, were the exponential function can be approximated by it linear term, $\left(\frac{4\delta g\gamma}{\pi}\right)^2 \tau_{\mathrm{intra}} p_{\mathrm{inter}} D_{\mathrm{inter}} \ll 1$. The dotted line is the difference between Ψ and the dashed line. It describes the decay by $p_{\mathrm{inter}} D_{\mathrm{inter}}$. The figure describes a monopolar rectangular gradient pulse with the width δ. Therefore, the factor $4/\pi$ due to bipolar sine-shaped gradient pulses is omitted.

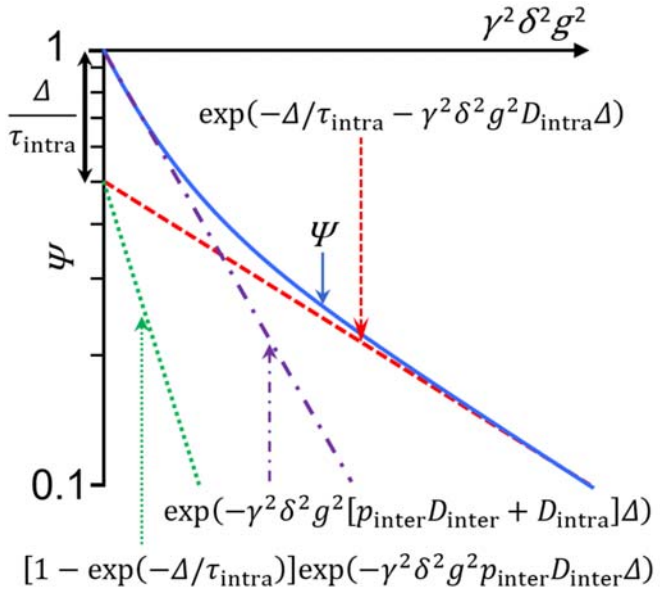

Fig. S9. Decay curve after Eq. (5) and some linear approximations. Part of the figure was taken from Ref. [10]. The special case $\tau_{\mathrm{intra}} = 2\Delta$ is considered.

6. Supplementary MD results and Talu results

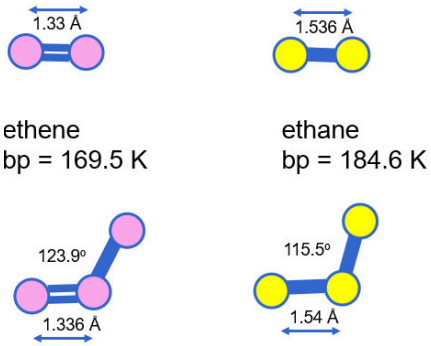

Fig. S10. Simulations for different temperatures.

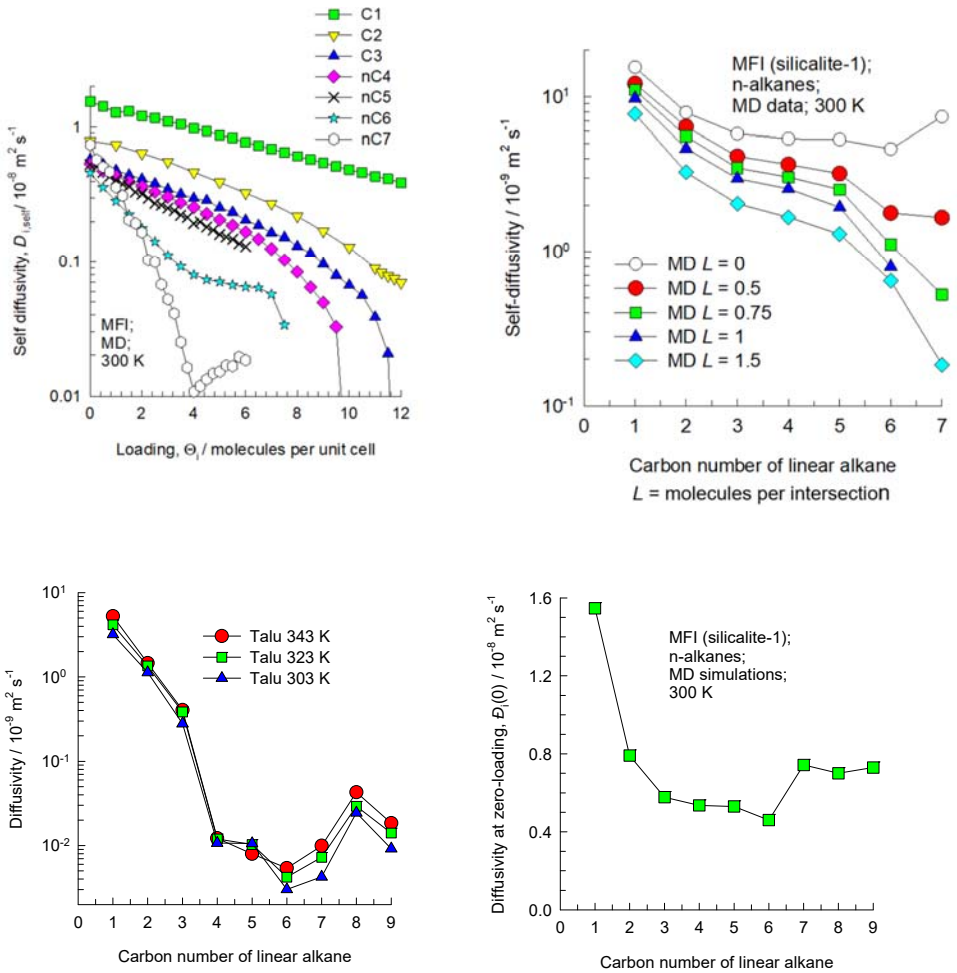

Fig. S11. Summary of MD simulation data [11-14] on self-diffusivities of *n*-alkanes in MFI zeolite at 300 K on the top, and experimental data of Talu et al. [15] for the chain length dependence of diffusivities of *n*-alkanes in MFI zeolite on the bottom. The Talu data were obtained from membrane permeation experiments.

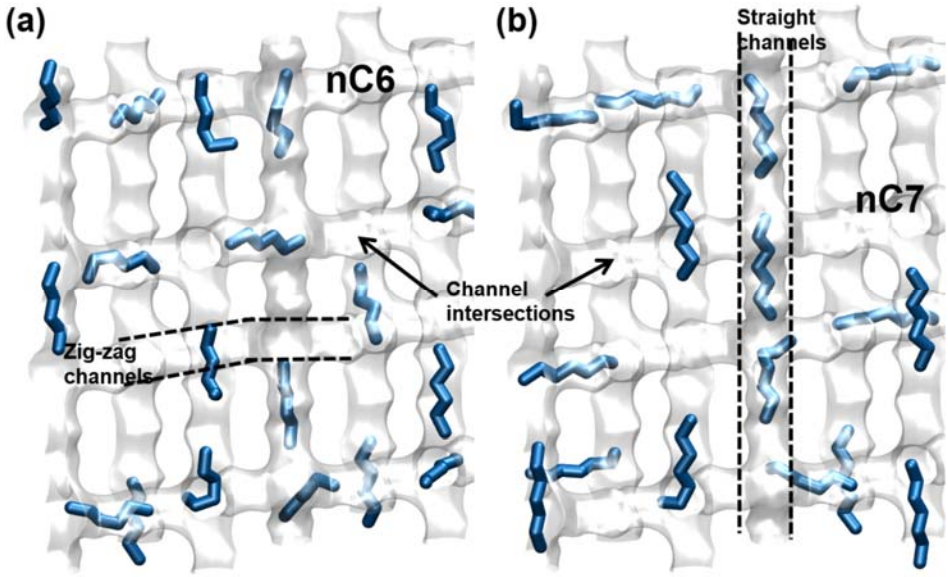

Fig. S12. Computational snapshots [16] of *n*-hexane and *n*-heptane in MFI zeolite.

References

[1] C.A. Fyfe, J.H. O'Brien, H. Strobl, Nature 326 (1987) 281-283.

[2] M. Hesse, H. Meier, B. Zeeh, Spectroscopic Methods in Organic Chemistry, 2th ed., Thieme, Stuttgart, New York, 2008.

[3] C. Chmelik, D. Freude, H. Bux, J. Haase, Microporous Mesoporous Mater. 147 (2012) 135-141.

[4] E.F. Meyer, D.G. Stroz, J. Am. Chem. Soc. 94 (1972) 6344-&.

[5] J.E. Tanner, J. Chem. Phys. 52 (1970) 2523-2526.

[6] R.M. Cotts, M.J.R. Hoch, T. Sun, J.T. Markert, J. Magn. Reson. 83 (1989) 252-266.

[7] D.H. Wu, A.D. Chen, C.S. Johnson, J. Magn. Reson. Ser. A 115 (1995) 260-264.

[8] M. Fernandez, J. Kärger, D. Freude, A. Pampel, J.M. van Baten, R. Krishna, Microporous Mesoporous Mater. 105 (2007) 124-131.

[9] U. Hong, J. Kärger, R. Kramer, H. Pfeifer, G. Seiffert, U. Müller, K.K. Unger, H.B. Luck, T. Ito, Zeolites 11 (1991) 816-821.

[10] J. Kärger, H. Pfeifer, W. Heink, Advances in Magn. Reson. 12 (1988) 2-89.

[11] R. Krishna, J.M. van Baten, Chem. Eng. Technol. 30 (2007) 1235-1241.

[12] R. Krishna, J.M. van Baten, Microporous Mesoporous Mater. 109 (2008) 91-108.

[13] R. Krishna, J.M. van Baten, Microporous Mesoporous Mater. 107 (2008) 296-298.

[14] R. Krishna, Microporous Mesoporous Mater. 185 (2014) 30-50.

[15] O. Talu, M.S. Sun, D.B. Shah, A.I.Ch.E.J. 44 (1998) 681-694.

[16] R. Krishna, J. Phys. Chem. C 113 (2009) 19756-19781.